Chaperone-assisted cryo-EM structure of *P. aeruginosa* PhuR reveals molecular basis for heme uptake

Paweł P. Knejski[1,2,4,†], Satchal K. Erramilli[1,†,*], and Anthony A. Kossiakoff[1,3,*]

[1]Deparment of Biochemistry and Molecular Biology, The University of Chicago, Chicago, IL, USA
[2]Laboratory of Medical Biology, Faculty of Biotechnology, University of Wrocław, Wrocław, Poland
[3]Institute for Biophysical Dynamics, The University of Chicago, Chicago, IL, USA
[4]Present address: Department of Biology, Institute of Molecular Biology and Biophysics, ETH Zurich, Zurich, Switzerland

[†]Equal contribution
*Correspondence should be addressed to: koss@bsd.uchicago.edu and satchal@gmail.com.

SUMMARY

Pathogenic bacteria, such as *Pseudomonas aeruginosa*, depend on scavenging heme for the acquisition of iron, an essential nutrient. The TonB-dependent transporter (TBDT) PhuR is the major heme uptake protein in *P. aeruginosa* clinical isolates. However, a comprehensive understanding of heme recognition and TBDT transport mechanisms, especially PhuR, remains limited. In this study, we employed single-particle cryogenic electron microscopy (cryo-EM) and a phage display-generated synthetic antibody (sAB) as a fiducial marker to enable the determination of a high-resolution (2.5 Å) structure of PhuR with a bound heme. Notably, the structure reveals iron coordination by Y529 on a conserved extracellular loop, shedding light on the role of tyrosine in heme binding. Biochemical assays and negative-stain EM demonstrated that the sAB specifically targets the heme-bound state of PhuR. These findings provide insights into PhuR's heme binding and offer a template for developing conformation-specific sABs against outer membrane proteins (OMPs) for structure-function investigations.

KEYWORDS

Phage display; synthetic antibodies; outer membrane proteins; TonB-dependent transporters; heme transport; cryo-EM; pathogenic bacteria

INTRODUCTION

TonB-dependent transporters (TBDT) are integral outer membrane (OM) proteins found in Gram-negative bacteria. Outer membrane proteins (OMPs) play vital roles in the acquisition of essential nutrients that are either too large or scarce to be taken up by simple diffusion through the semi-permeable OM, including iron, heme, vitamin B12, and carbohydrates[1,2]. These OM transporters form transiently open channels that enable the selective uptake of substrates into the periplasmic space while preserving the integrity of the outer membrane[2,3]. TBDTs are physically coupled to an inner membrane energy transducing complex, which allosterically powers nutrient uptake into the periplasm using the proton motive force, the details of which are not completely understood[4–6].

Iron is one such essential nutrient for the survival and virulence of many bacterial pathogens, and hence iron complexes, including heme, constitute the majority of substrates taken up by TBDTs[3,7,8]. *Pseudomonas aeruginosa* is an opportunistic pathogen with at least two heme uptake systems: the heme assimilation system (*has*) and the *Pseudomonas* heme uptake (*phu*) system[9,10]. The *has* operon encodes a secreted hemophore, HasA, which extracts heme from environmental hemoglobin and delivers it to an OM TBDT, HasR[11,12]. The *phu* operon encodes an 82-kDa OM TBDT, PhuR, that captures heme directly from the extracellular milieu[9,13]. Substrate binding to each TBDT triggers a signal transduction cascade across the membrane, with the TonB-ExbB-ExbD complex catalyzing heme uptake into the periplasmic space. The presence of multiple systems, common in Gram-negative bacteria, thus provide *P. aeruginosa* a significant advantage in competing for this limited resource within the host environment[10]. Moreover, iron acquisition is known to be essential for biofilm formation[13].

It is in this setting that PhuR appears to play a crucial role. Transcriptome analyses from *P. aeruginosa* clinical lung isolates show PhuR is the major OM heme receptor in clinical infections, rather than HasR, with mutations in the *phu* operon resulting in increased PhuR expression levels[14]. *P. aeruginosa* Δ*phuR* knockout strains are unable to utilize heme as well as the wild-type, suggesting an essential role for PhuR[9]. These observations suggest potential physiological roles for each system, with HasA/HasR thought to functional primarily in heme sensing while PhuR is mainly involved in uptake[13]. Biochemical analysis of PhuR suggest a His-Tyr pair is involved in heme binding, but limited structural evidence is currently available for heme recognition by TBDTs[10].

To better understand the structural basis for heme recognition by PhuR, we endeavored to determine its three-dimensional structure using single particle cryogenic electron microscopy (cryo-EM). Due to the current size limitations of cryo-EM, we assisted our efforts by the generation of a high affinity synthetic antibody (sAB) specific for PhuR using a robust phage display technology developed in our group[15–18]. These sABs have demonstrated utility as fiducial markers in cryo-EM[19–22]. We determined a 2.5 Å resolution cryo-EM structure of PhuR using one sAB from this campaign, termed sAB11. Our structure contains bound heme and Lipid A molecules, both likely co-purified with PhuR, providing structural insights into heme recognition and lipid interactions with OM proteins. In contrast with a previous study, our structure shows Y529 coordinates heme near the top of the extracellular domain[10]. We further demonstrate that sAB11 is conformation-specific by denaturing and refolding PhuR to produce the apo state, which can only form a complex with the sAB when heme is bound to it. Our results provide insight into

substrate recognition by TBDTs and serve as a template for the generation of biochemical tools against similar OMPs.

RESULTS

Purification of *P. aeruginosa* PhuR and synthetic antibody generation

We recombinantly expressed *Pseudomonas aeruginosa* PhuR using an N-terminal hexa-histidine tag and by replacing the native signal peptide (spanning residues 1-25) with a PelB sequence[23]. PhuR was expressed in *E. coli* C41 (DE3) cells, solubilized from outer membranes using DDM, and purified by immobilized metal affinity chromatography (IMAC). DDM-solubilized PhuR was then analyzed by gel filtration chromatography, and eluted as a highly pure single peak from the column (**Supplemental Fig. 1A)**. Circular dichroism (CD) spectroscopy confirmed the purified detergent-solubilized protein was primarily comprised of β-sheets, and thermal denaturation experiments showed purified PhuR has a melting temperature (T_m) of 71°C (**Supplemental Fig. 2**).

To overcome current cryo-EM size limitations, we screened a highly diverse and fully synthetic antibody (sAB) library to obtain binders specific for recombinant PhuR[24]. PhuR was reconstituted into lipid-filled nanodiscs (**Supplemental Fig. 1B**) formed using chemically biotinylated membrane scaffold protein (MSP) E3D1, and five rounds of biopanning were performed using a well-established selection protocol[17,18,25]. We identified over 70 unique PhuR-specific binders after the initial validation, and selected the 18 best candidates from this pool for subcloning, expression, purification, and further analysis (**Fig. 1A-B, Supplemental Table 1**). This set was then filtered based on sAB affinities for PhuR and complex formation efficiency (**Fig. 1C**, **Supplemental Table 2**).

Based on this analysis, sAB11, which has an EC_{50} of ~9 nM, was chosen for structure determination of PhuR by fiducial-assisted cryo-EM.

sAB-assisted single-particle cryo-EM enables high-resolution structure determination of PhuR

We initially performed cryo-EM single-particle analysis (SPA) with the PhuR-sAB11 complex reconstituted into nanodiscs. However, due to empty nanodisc contamination and the presence of few intact complexes, a high-resolution cryo-EM map could not be obtained in this condition (data not shown). To improve the sample quality, detergent-solubilized PhuR was reconstituted instead into amphipols, which have demonstrated utility in cryo-EM SPA of membrane proteins[26]. Amphipol-reconstituted PhuR similarly forms a stable complex with sAB11. To improve the cryo-EM data, we also utilized a nanobody (Nb) that binds with high-affinity to the sAB hinge region and functions as an additional fiducial marker for cryo-EM SPA[27]. We obtained high-quality grids of the tripartite complex and collected cryo-EM data (**Supplemental Fig. 3A**).

This sample enabled the structure determination of the PhuR-sAB11-Nb complex to an overall nominal resolution of 2.5 Å, with most of the PhuR molecule resolved to ~2.4 Å (**Fig. 2A**, **Supplemental Fig. 3A-C**). The majority of the cryo-EM data contained monomeric PhuR; however, it also included an antiparallel dimer form of PhuR, which could be readily segregated into a separate particle class. The two distinct particle classes are apparent from two-dimensional class averages, and the intact complexes of PhuR with sAB11 and Nb are clearly visible (**Supplemental Fig. 3A**). The antiparallel PhuR dimer similarly contained two molecules of the sAB11-Nb complex and had a nominal 3

Å resolution. Given the non-physiological nature of the dimer and overall lower resolution, it was not further analyzed.

For initial cryo-EM density fitting, we started with a model of monomeric PhuR comprising residues 47-578 and 585-764 (**Supplemental Table 3, Supplemental Fig. 4)** using AlphaFold[28]. The final experimental structure shows PhuR is an all-next neighbor antiparallel 22-stranded β-barrel outer membrane protein (OMP), with the strands all tilted ~45° to the normal of the membrane (**Fig. 2B**) and an N-terminal plug domain located within the barrel. These structural features are conserved amongst TonB-dependent transporters (TBDT)[2,3]. PhuR is overall asymmetric in shape, with strands 6-9 forming a 74 Å height wall along one side of the barrel that extends well into the extracellular domain, and shorter wall on the other side of the barrel (**Fig. 2B**). We identified density along the shorter outer wall of the barrel, near strands 16-20, that was tentatively assigned as a portion of a lipopolysaccharide (LPS) molecule that was present during purification (**Fig. 2A-B**). We could resolve the Lipid A and first KDO sugar in this density, while the rest of the LPS was not present in the cryo-EM map (**Fig. 2C-D**). The structure revealed the Lipid A C-1 and C-4' phosphate headgroups likely interacting with PhuR residues K721 and R670, respectively, while a number of conserved hydrophobic residues appear to form van der Waals interactions with the six fatty acid tails (**Fig. 2E**). The headgroup interactions are typically conserved in LPS binding sites, supporting this interpretation[21].

Residues 47-166 form the N-terminal plug domain, a hallmark feature of TBDT that is critical for sensing and uptake of the ligand[29,3]. The N-terminal residues prior to the plug, which exclude the processed signal peptide but potentially include the Ton box, were not resolved[2]. These residues are resolved in some structures, including BtuB (PDB

ID 1NQH), but has also been shown to be more dynamic when substrates are bound in other TBDTs[6,30,31]. The rest of the plug was well resolved and contained the conserved fold typical of β-barrel TBDTs[3]. The core of this domain is a 4-stranded β-sheet tilted with respect to the plane of the membrane, while the remainder is composed of short helices and long loops projecting upwards towards the extracellular surface (**Fig. 2B**).

The periplasmic loops, or turns as they are conventionally described, of PhuR are all relatively short. The longer of the extracellular loops, many composed of well-structured elements, create a large vestibule leading to the hydrophilic interior of the barrel, which is 40 Å wide and occluded by the plug in our structure. We could confidently model all of these segments except for the tip of the extracellular loop connecting strands 15 and 16 (residues 579-584), which appears to be disordered.

The sAB11 interacts extensively with the extracellular vestibule of PhuR, primarily through complementarity-determining regions (CDRs) H2, H3, and L3. The contacts are formed by both hydrogen bond and van der Waals interactions with the extracellular loops and bury ~1000 $Å^2$ of surface area at the interface (**Fig. 2F**). The 16-residue long sAB CDR-H3 forms a blunt wedge, packing against an extracellular conserved loop (CL). This loop contains the conserved FRAP/PNPNL motif that spans residues 510-513 and 533-537, respectively, and the β-strands that comprise the taller edge of the barrel (**Fig. 2B**). The FRAP motif diverges somewhat in PhuR, where it is actually FRTP. Hydrogen bond interactions mediate many of the contacts between sAB11 and PhuR, including CDR-H3 residue S114 with CL residue Q526, HC residues Y57 and Y107 with PhuR D279, and H3 residue Y111 with R398. The latter two PhuR residues are located on the tall edge of the barrel within extracellular loops and β-strands, respectively.

PhuR cryo-EM map revealed heme bound to extracellular site

We unexpectedly observed well-resolved non-protein cryo-EM density in an extracellular cavity near the sAB epitope, which we readily modeled as a bound heme molecule that co-purified with PhuR (**Fig. 2G, Fig. 3A-C**). The heme molecule is bound through multiple sets of interactions with the protein. The heme iron is coordinated through the hydroxyl group of Y529, which is located on the structured extracellular CL between strands 13-14 that forms a β-turn and contacts sAB11 CDR-H2. The distance between the Y529 hydroxyl oxygen and heme iron (1.9 Å) is consistent with the typical Fe-O distance observed in heme-coordinating tyrosine residues. The aforementioned conserved FRTP (FRAP) and PNPNL motifs flank the conserved Y529, with the CL forming a lid over the extracellular heme-binding site to create a predominantly hydrophobic binding pocket near the outermost surface of PhuR (**Fig. 3B, D-F**). Several nearby residues stabilize heme in this pocket, including R353 and R355, which form hydrogen bonds with the propionate sidechains, F522 and F588 through π-π stacking, and L416, I531, V735, and L741 through van der Waals interactions. At the tip of a 24-amino acid long loop rising upwards from the plug domain are residues F116, P119, and Y120, which also interact with heme, thus connecting the extracellular binding site with the region of PhuR responsible for partnering with inner membrane energy-transducing complexes to facilitate ligand uptake. While the conformation of the plug domain is similar to those observed in β-barrel OMP structures in their apo states, such as BtuB (PDB ID 1NQG) and ShuA (3FHH), the orientation and substrate interactions of this loop are distinct in our PhuR structure **(Fig. 3G-H**)[30,32]. Combined with the lid formed by the CL,

this plug loop sandwiches the heme into its binding site. This is structurally similar to the HasA-HasR complex (3CSL), where the heme iron is coordinated after transfer from HasA by HasR to residues H603, which resides in the same extracellular loop, and H189 from the plug loop[12]. In the BtuB structure with bound cyanocobalamin (1NQH), the plug, including the homologous loop, interacts extensively with the substrate, in part due to the binding site residing at a lower position within the barrel and due to the substrate size[30].

Biochemical and mutational analyses previously reported that the conserved residues Y519, located on the CL following the FRAP motif, and H124, on the plug domain, are involved in heme coordination[10]. In the structure, Y519 is pointing away from heme, with the hydroxyl positioned towards the extracellular space. H124, which is part of the same plug domain loop that contacts the heme, is located too far, ~16 Å, to participate in binding (**Fig. 3D-F**). Neither of these is located near the cavity where heme is observed to be bound (**Fig. 4A**). A second, much smaller cavity spans the space between Y519 and H124 located below the observed heme binding site (**Fig. 4A-B**), with a narrow channel connecting the two cavities (**Fig. 4C-E)**. There was no cryo-EM density in the second cavity corresponding to heme, which is not surprising since the cavity would have to expand significantly through substantial conformational changes to accommodate it. We posit that these potential conformational differences might be induced from differences in the expression and purification protocols.

Refolded PhuR is active for heme binding but resistant to structure determination

To better understand the conformational changes of PhuR associated with heme binding, we isolated the apo state by expressing into inclusion bodies PhuR without the

signal peptide. This method is well-established for obtaining high yields of β-barrel outer membrane proteins for structural studies[23]. PhuR was denatured using 5 M urea, applied to an IMAC column, refolded by slow buffer exchange in the presence of DDM, and subsequently purified. Gel filtration chromatography was used to separate folded and unfolded proteins. Peak fractions containing folded PhuR were pooled and analyzed using CD spectroscopy, which established that refolded PhuR is composed predominantly of β-sheet secondary structure (**Supplemental Fig. 2**). Thermal denaturation of refolded PhuR showed a T_m of 65°C, 6°C lower than the natively expressed version. Spectroscopic analysis of refolded PhuR suggested heme was not present in the sample (data not shown). Using a spectrophotometric assay, we determined refolded PhuR binds hemin with an affinity of ~12.5 μM, demonstrating that the protein is active (**Fig. 5A**).

To assist in structure determination by cryo-EM, the ~70 sABs obtained from the native PhuR selection were tested for binding to refolded PhuR. None of these sABs showed measurable binding to the refolded protein, including sAB11. We subsequently reconstituted refolded PhuR into chemically-biotinylated nanodiscs and biotinylated amphipols and performed phage display as described earlier. However, no high-affinity specific binders to refolded PhuR were identified in these selections. We then attempted to determine the structure of refolded PhuR reconstituted into both nanodiscs and amphipols, but were unable to obtain a high-quality cryo-EM reconstruction (data not shown). These results suggest that in the absence of heme, which was not observed using spectrophotometry, and LPS, which is likely not bound to proteins refolded from inclusion bodies, parts of PhuR are highly flexible and dynamic, preventing both sAB

generation and cryo-EM structure determination. Relatedly, in several crystal structures of β-barrel OMPs, density for these loops is often missing due to flexibility, and it is known these regions are essential for transport[30,32–35].

To better understand the mode of heme binding, we attempted to form a complex between sAB11 and refolded PhuR in the presence of hemin. Amphipol-reconstituted refolded PhuR was incubated with 50 µM hemin, and subsequently sAB11 was added to this solution. The complex was purified by gel filtration chromatography (**Fig. 5B**). Analysis of the peak fractions by SDS-PAGE showed bands for both PhuR and sAB11 when hemin was present (**Fig. 5C**). The PhuR-sAB11 complex was not formed when hemin was not present. This complex was subsequently analyzed by negative-stain electron microscopy (ns-EM). Two-dimensional ns-EM class averages clearly showed the sAB bound to refolded PhuR in a manner similar to native PhuR (**Fig. 5D-E**). These experiments demonstrated both that sAB11 is specific to the heme bound conformation of PhuR, and that the mode of heme binding could be recapitulated by the addition of hemin to the refolded PhuR preparation.

DISCUSSION

Iron is an essential nutrient for all bacteria, and establishing a ready source is indispensable for growth and virulence for a number of pathogens[3,7]. PhuR is a central player in heme acquisition in *Pseudomonas aeruginos*a, and is particularly important in clinical strains of this nosocomial pathogen[9,10,13]. It is thus potentially an attractive target for therapeutics, and understanding its structure-function relationship is key for the design and development of drugs against this TonB-dependent transporter.

We describe here the first experimental structure of PhuR using single particle cryo-EM. To overcome the current size limitation of cryo-EM for this 82-kDa integral membrane protein, we generated a high affinity sAB, sAB11, using a phage display technology developed in our group for nanodisc-reconstituted membrane proteins[15–18]. High-quality cryo-EM data was obtained for the complex of PhuR with sAB11, which facilitated accurate model building and detailed interpretation at 2.5 Å resolution

The overall architecture is consistent with other TBDTs, with PhuR composed of 22 antiparallel β-strands and an N-terminal plug domain. Long extracellular loops form a large vestibule, which unexpectedly contained a bound heme molecule. The cryo-EM density contained well resolved features, enabling model building with high accuracy the interactions facilitating heme binding and recognition with high accuracy. The heme is coordinated by a Fe-O bond formed between the heme iron and PhuR Y529 hydroxyl. This observation adds to a growing body of knowledge regarding the role of tyrosine in heme binding for a variety of proteins[10,13,36]. This result was also unexpected based on an earlier biochemical and mutational analysis, which suggested key roles for Y519 and H124[10]. We identified these residues proximal to a second smaller cavity located lower in the barrel. We observed no class averages in the data that might suggest PhuR populates additional minor substates aside from the major one described above. Thus, whether this second cavity represents a potential pathway to an intermediate state in heme transport remains an open question.

To better understand the conformational changes associated with heme binding, we denatured and refolded PhuR to obtain its apo state, and determined its ability to bind hemin with low micromolar affinity. In the hemin bound form, refolded PhuR was able to

form a complex with sAB11, demonstrating the conformation-specificity of this reagent. Negative-stain EM analysis confirmed the binding of sAB11, showing we could recapitulate its binding mode using the refolding preparation together with added hemin. This result confirms that the heme-bound form was the predominant form in solution when the initial biopanning was performed. We also attempted to determine the structure of refolded apo PhuR, but were unsuccessful in obtaining sABs specific to it and determine a cryo-EM structure in the absence of any such fiducial marker. We posit that PhuR, in the absence of both heme and, because it is refolded from inclusion bodies, LPS is too flexible, and that these factors are essential for stability and restricting conformational dynamics of the extracellular loops that enable high affinity sAB generation. Indeed, refolded PhuR has a reduced T_m compared with the native, holo state that was isolated after expression into *E. coli* outer membranes. Additionally, in the absence of these conformationally stable loops, the β-barrel structure in amphipols did not have sufficient features to enable the alignment of images during cryo-EM data processing.

Overall, our findings shed light on the structural features of PhuR and its interactions with heme, adding to the growing body of knowledge of how TBDTs initially bind and recognize their transported substrates. Future studies could further investigate the functional relevance of heme binding to the observed site, the role of the potential second binding site, and the relevance of both to the transport mechanism of PhuR. Alternative strategies could enable the structure determination of additional functionally-relevant states of PhuR. These could include mutational scanning to identify residues involved in substrate transport and the interaction with TonB. Further, synthetic antibodies, such as those generated for these studies, with inhibitory activities against

TBDTs involved in nutrient uptake could be developed into powerful new classes of therapeutics against nosocomial pathogens such as *P. aeruginosa*[37]. This study thus provides a template for the generation of such binders.

ACKNOWLEDGEMENTS

We would like to thank Khuram Ashraf, Tomasz Gawda, Duy P. Hua, Marc André Leibundgut, Julia Marcińska, Somnath Mukherjee, Nicholas Noinaj, Zachary P. Schaefer, and Michał Śmiga for their critical feedback, helpful discussions, and kind assistance during the course of this study and in the preparation of this manuscript. We thank Jotham Austin II, Tera Lavoie, James R. Fuller, Yimei Chen, and the rest of the staff at the University of Chicago Advanced Electron Microscopy facility for help with cryo-EM data collection. We thank Elena Solomaha and the University of Chicago Biophysics core for their help with CD spectroscopic experiments. This work was supported by NIH grant R01GM117372 to A.A.K.

AUTHOR CONTRIBUTIONS

PPK and SKE conducted the experiments. SKE and AAK designed the research. All the authors analyzed the results, wrote, and edited the manuscript.

DATA AVAILABILITY

The raw movie frames have been deposited into the Electron Microscopy Public Image Archive (EMPIAR), with accession code EMPIAR-11627. The cryo-EM density maps have been deposited into the Electron Microscopy Data Bank (EMDB, accession code EMD-41255). The coordinate file has been deposited in the Protein Data Bank (PDB, accession code 8THE). Synthetic antibodies generated in this study will be made available upon request.

METHODS

Expression and purification of PhuR from native membranes

The codon-optimized PhuR gene from *Pseudomonas areuginosa* PAO1 strain lacking the native signal sequence (MPLSPPFALRPCLALLLLSPSLALA) was synthesized and cloned into the expression vector pET20b(+), which contains an N-terminal pelB signal sequence and hexahistidine tag (Genscript). The construct was transformed into chemically competent C41 (DE3) cells (Lucigen) and plated after heat shock and recovery on LB agar supplemented with ampicillin. Colonies were allowed to grow with an overnight incubation at 37°C. The following day, a single colony was used to inoculate 30-mL of LB liquid media with 100 µg/mL ampicillin and grown overnight with shaking. The inoculum was transferred to 3 L of TB media supplemented with ampicillin and 0.4% (w/v) glycerol in baffled Fernbach flasks (Corning). Cultures were grown to mid-log phase (OD_{600} of 0.6-0.8), subsequently induced with 100 µM IPTG (RPI Chemicals), and proteins were expressed for 4 hours at 37°C. Cells were harvested by centrifugation and frozen until further use.

For purification, cell pellets were resuspended in lysis buffer (25 mM Tris, pH 7.4, 150 mM NaCl with 1 mM PMSF (Sigma)) and homogenized (IKA Labs). Cells were lysed by two cycles of sonication (Branson Sonifier; 40% amplitude, 1.5-min cycle of 1-s on/1-s off). Membranes were solubilized by the addition of 1% n-dodecyl-β-D-maltopyranoside (DDM, Anatrace) followed by a one-hour incubation at 4°C with nutation. Insoluble material and cellular debris were removed by ultracentrifugation at 40,000 RPM for 45 minutes at 4°C using a Ti45 fixed-angle rotor (Beckman-Coulter). The resulting supernatant was supplemented with NaCl and imidazole to final concentrations of 500

and 20 mM, respectively, and subsequently applied to a 5-mL HisTrap column (GE Healthcare) pre-equilibrated with wash buffer (25 mM Tris, pH 7.4, 500 mM NaCl, 20 mM imidazole, 0.1% DDM). Following batch binding for one hour, the column was washed using a linear imidazole gradient (20-500 mM) formed by mixing wash buffer with elution buffer (wash buffer with 500 mM imidazole) on a fast protein liquid chromatography system (FPLC, ÄKTA) with fractionation and monitored using A_{280}. Fractions containing protein were analyzed by SDS-PAGE, and PhuR-containing fractions were pooled and concentrated using 50-kDa MWCO centrifugal filters (Amicon). The resulting sample was dialyzed overnight in 25 mM Tris, pH 7.4, 150 mM NaCl buffer. The dialyzed sample was subsequently purified by size exclusion chromatography using a Superdex200 HiLoad 16/600 column (GE Healthcare). Fractions were analyzed by SDS-PAGE gel, and PhuR-containing fractions were pooled, concentrated, supplemented with 10% glycerol, flash frozen in liquid nitrogen, and stored at -80°C until further use.

Expression and purification of PhuR from inclusion bodies

The codon-optimized PhuR gene described above was also cloned into vector pET28b(+) (Genscript), which contains an N-terminal hexahistidine tag but lacks a signal sequence. A similar transformation and expression protocol was used, except substituting kanamycin (50 µg/mL) for ampicillin. Cells were harvested, homogenized, and lysed as described above. Inclusion bodies and other insoluble material were collected by centrifugation at 10,000×g at 4°C for 10 minutes. The resulting pellet was washed twice with denaturing buffer (25 mM Tris, pH 7.4, 500 mM NaCl, and 5 M Urea) and incubated for one hour at RT with nutation. The suspension was centrifuged at 10,000×g at 4°C for

20 minutes. The supernatant was collected, passed through at 0.2 µm filter, and subsequently injected onto a 5-mL HisTrap column (GE Healthcare) connected to an ÄKTA FPLC system. Prior to injection DDM was added to the supernatant at a final concentration of 0.1% (w/v). PhuR was refolded by slow exchange of buffer to remove urea using refolding buffer (25 mM Tris, pH 7.4, 500 mM NaCl, 0.1% DDM). Following refolding, PhuR was purified using a linear gradient of imidazole as described above for native PhuR. Fractions were analyzed by SDS-PAGE, and those containing PhuR were pooled, concentrated, and injected onto a Superdex200 HiLoad 16/600 SEC column (GE Healthcare) to separate folded and unfolded proteins. The SEC was performed using SEC buffer: 25 mM Tris, pH 7.4, 150 mM NaCl, and 0.02% DDM. Fractions were analyzed by SDS-PAGE using the heat modifiability property to assess whether PhuR was folded or unfolded[38]. Fractions containing folded PhuR pooled, concentrated, and stored as described above until further use.

Circular dichroism and thermal denaturation assays

Far UV CD spectra were measured in a wavelength range of 180-260 nm using a Jasco J-1500 CD Spectrometer with a cell path length of 1 cm and a protein concentration of 5 µM in SEC buffer. The spectra were recorded using triplicate scans. For thermal denaturation studies, a fixed wavelength of 222 nM was monitored and simultaneous OD and CD scans were measured from 26 to 98°C. Temperature was increased by steps of 2°C with 3-min incubation periods between spectral measurements. Data fitting and analysis were performed using Spectra Manager (Jasco) and Prism 9.0 (GraphPad).

Nanodisc reconstitution

MSP E3D1 was expressed and purified as previously described, including removal of the polyhistidine tag by digestion with TEV protease[39]. For phage display purposes, MSP was chemically biotinylated as previously described[17]. DDM-solubilized PhuR was mixed with either biotinylated or non-biotinylated E3D1 and total *E. coli* lipid extract (Avanti) in a 1:6:480 molar ratio. A lipid solution was prepared as previously described prior to incubation with the reconstitution mixture[40]. Empty nanodiscs for phage display were also prepared by mixing either biotinylated or non-biotinylated E3D1 with lipids in a 1:130 molar ratio. To form nanodiscs, detergent was removed by overnight incubation with activated Bio-Beads SM-2 (Bio-Rad). For purification of PhuR-containing nanodiscs, the reconstitution mixture was transferred from Bio-Beads to Ni-NTA resin (Qiagen). IMAC was performed using buffers similar to those described above, except without detergent. Fractions containing PhuR nanodiscs were pooled, concentrated, and injected onto a Superdex200-increase 10/300 GL SEC column (GE Healthcare) pre-equilibrated with nanodisc buffer: 25 mM Tris, pH 7.4, 150 mM NaCl. Fractions containing PhuR nanodiscs were pooled, concentrated, flash frozen in LN2, and stored at -80°C until further use.

Identification of PhuR-specific sABs using phage display

For sAB screening, biotinylated nanodiscs containing PhuR were used. Selections were performed using PhuR both from native and refolding conditions. Prior to phage display, the efficiency of capture on streptavidin-coated paramagnetic beads (Promega) was evaluated as described before. Biopanning was performed using phage display sAB

Library E in selection buffer (25 mM Tris, pH 7.4, 150 mM NaCl, 1% BSA) according to previously described protocol[17–19]. In the first round, biopanning was performed manually using 400 nM of PhuR nanodiscs immobilized onto paramagnetic beads by one-hour incubation at RT with Library E. Following three washes with selection buffer, beads enriched for phage displaying PhuR-specific sABs were used to directly infect log-phase *E. coli* XL-1 Blue bacteria. Following a 20-min infection, 2×YT media supplemented with ampicillin (100 µg/mL) and M13-KO7 helper phage (10^9 PFU/mL) was added and phage were amplified overnight. To increase the stringency of sAB selection, four additional rounds of biopanning were performed by decreasing PhuR concentrations in a stepwise manner: 200, 100, 50, and 25 nM. For rounds 2-5, the amplified phage pool from each preceding round was using as the input, and biopanning was performed semi-automatically using a Kingfisher magnetic beads handler (Thermo Fisher Scientific). The phage pools for rounds 2-5 were pre-cleared with 200 µL of streptavidin beads to remove non-specific binders. In all rounds, a tenfold molar excess of non-biotinylated E3D1 nanodiscs were used as soluble competitors to remove MSP-specific sABs. Finally, for rounds 2-5 phage particles were eluted from magnetic beads by a 15-min incubation step with 1% Fos-choline-12 (Anatrace) prepared in buffered saline.

Initial validation using single-point phage ELISA

Colonies of E. coli XL-1 Blue bacteria containing individual phagemid clones from round 5 of phage display were used to inoculate 400 µL of 2×YT media supplemented with ampicillin (100 µg/mL) and M13-KO7 helper phage (10^9 PFU/mL). Phage were amplified overnight in 96-well deep well blocks at 37°C with shaking at 280 RPM.

Amplified phage were diluted into ELISA buffer (selection buffer with 0.5% BSA) and then tested against PhuR-loaded or empty biotinylated E3D1 nanodiscs. All ELISA experiments were performed on 96-well ELISA plates (Nunc) coated overnight with 2 µg/mL neutravidin and blocked for at least two hours with selection buffer. ELISA were performed as previously described and bound phage were detected with TMB substrate (Thermo Fisher Scientific) following a 30-min incubation with HRP-conjugated anti-M13 monoclonal antibody (Antibody Design Laboratories)[19]. Absorbance was measured at 450 nm following quenching with 1 M HCl. Wells containing empty biotinylated E3D1 nanodiscs were used to determine non-specific binding. Specific binders were determined based on their signal/background ratio.

sAB expression and purification

Selected clones based on phage ELISA were sequenced at the University of Chicago Comprehensive Cancer Center DNA Sequencing facility. Unique clones were sub-cloned into the sAB expression vector pRH2.2 (kind gift of S. Sidhu) using the In-Fusion Cloning Kit (Takara Bio). The best candidates (based on highest ELISA signals) were expressed and purified as previously described[19].

Assessment of sAB binding affinity for PhuR

ELISA were performed using purified sABs to estimate apparent binding affinities as previously described. ELISA plates were prepared as above for phage ELISA. 25 nM of either PhuR-loaded or empty biotinylated nanodiscs were immobilized onto wells. Binding was assessed using 3-fold serial dilutions of sABs starting from 3 µM maximum

concentrations. Bound sABs were detected with TMB substrate following a 30-min incubation with HRP-conjugated recombinant protein L (Pierce). Reactions were quenched with 1 M HCl and absorbance was measured at 450 nm. The signals were background subtracted and normalized A_{450} values were plotted against the $\log_{10}$ sAB concentrations. EC_{50} values were then calculated in Prism 9 (GraphPad) using a variable slope model and assuming a sigmoidal dose response.

Amphipol (APol) reconstitution

APol A8-35 (Anatrace) was mixed with native or refolded PhuR in SEC buffer with DDM in a 1:10 PhuR/APol mass ratio. The solution was incubated on ice for 20 minutes, followed by the addition of Bio-Beads to remove DDM. Amphipol reconstitution was performed overnight at 4°C with nutation. The reconstitution mixture was then transferred from Bio-Beads, filtered using 0.2-µm centrifugal filter units, and injected onto a Superdex200-increase 10/300 GL column equilibrated with SEC buffer (without DDM). Fractions containing PhuR reconstituted into A8-35 were analyzed by SDS-PAGE, pooled, concentrated, and flash frozen until further use. An identical protocol, except using biotinylated A8-35 (Anatrace), was used to reconstitute refolded PhuR into biotinylated amphipols for phage display.

Heme binding studies

5-µM of protein solution in APols was prepared and added to a 96-well plate. Hemin solutions (Sigma) ranging from 1-50 µM were added to PhuR and incubated for 20 minutes at RT. The UV-Vis spectrum was recorded from 190-850 nm using a

Nanodrop One (Thermo Fisher Scientific). The background signal was subtracted from protein-heme wells using wells containing heme but not protein. Values at the Soret peak (410 nm) were plotted as a function of heme concentration and analyzed using nonlinear regression in Prism 9 (GraphPad).

PhuR complex formation with sAB11 and anti-sAB nanobody

Amphipol-reconstituted native PhuR was combined with a 2-fold molar excess of sAB11 and 3-fold molar excess of an anti-sAB nanobody, which was expressed and purified as previously described. Following a 20 minute incubation, the complex was loaded on a Superdex200-increase 10/300 GL column (Cytiva) in SEC buffer (without DDM). Fractions containing all complex components were pooled and concentrated.

Complexes with amphipol-reconstituted refolded PhuR with sAB11 and the anti-sAB nanobody were similarly formed and isolated, except for the addition of 50µM hemin prior to incubation with the sAB and nanobody.

Negative-stain electron microscopy

To determine sample quality and success of complex formation, purified proteins were diluted to 0.05 mg/mL and applied onto plasma-cleaned (Gatan Solarus) copper grids with a continuous carbon layer (Electron Microscopy Sciences). The grids were washed twice with droplets of water, and then blotted with Whatman 4 filter paper to remove the excess solution. The grids were stained with two applications of 1% uranyl formate (EMS), and again blotted. After drying, the grids were imaged using a FEI Spirit 120 kV microscope equipped with a digital CCD camera with 2k × 2k resolution using a

pixel size of 2.1 Å. In total, 30-50 images were collected for the native and refolded PhuR with and without sABs, using peak SEC fractions diluted into SEC buffer at the aforementioned concentration to prepare the ns-EM grids. Images were processed using Relion-3.0 to obtain two-dimensional class averages[41].

Single-particle cryo-EM vitrification and data collection

APol-reconstituted native PhuR complexes with sAB11 and the nanobody were concentrated to 2-5 mg/mL using a 100-kDa molecular weight cutoff concentration (Amicon). Prior to vitrification, 0.25% CHAPSO was added to improve the quality of vitreous ice during freezing and reduce denaturation and aggregation at the air-water interface. 3.5 µL of sample was applied to plasma-cleaned (Gatan Solarus) 1.2/1.3-µm UltrAuFoil grids (Quantifoil) and blotted using standard Vitrobot filter paper (Ted Pella, 47000-100) on both sides for 4 seconds using a Vitrobot Mark IV (Thermo Fisher Scientific) operating at 8°C and 100% humidity. The grids were immediately plunged after blotting into liquid ethane for vitrification. Cryo-EM images were collected at the University of Chicago Advanced Electron Microscopy Facility using a Titan Krios G3 electron microscope (Thermo Fisher Scientific) operating at 300 kV and equipped with a Gatan K3 direct detection camera and Energy Filter (BioQuantum). Automated data collection was done in CDS mode using the EPU software package. A total of 5,031 movies consisting of 50 fractions with a 60 e^-/Å total exposure were collected with a super-resolution pixel size of 0.534 Å, a calibrated pixel size of 1.068 Å, and a defocus range of -1.0 to -2.5 µm.

Cryo-EM data processing for PhuR-sAB11-nanobody complex

All data processing and visualization software used were part of the SBGrid collection except for cryoSPARC (v3.3)[42,43]. Movies were subjected to motion correction by MotionCor2 (v1.4.0) within the Relion-4.0-beta GUI[44,45]. CTF parameters were determined using GCTF (v1.06)[46]. Micrographs were filtered based on defocus values, astigmatism, resolution, and figure of merit, leaving 4,153 micrographs in the final set. Around 5 million particles were selected using the Laplacian-of-Gaussian (LoG) picker. The particles were extracted using a box size of 360 pixels and imported into cryoSPARC (v3.3). Several iterations of 2D class averaging were performed to remove junk particle. Particles were selected based on whether 2D classes contained monomers or antiparallel dimers of PhuR. These sets were independently and in parallel subjected to *Ab initio* reconstruction, classification using heterogeneous refinement, and non-uniform refinement, with the final particle sets containing 277,088 and 141,268 particles and producing monomer and dimer maps of 3.0 and 3.3 Å resolutions, respectively. The particle sets were exported to Relion for CTF refinement and Bayesian polishing using pyem, and then imported back to cryoSPARC for non-uniform refinement and local refinement using masks generated in Chimera around PhuR and the sAB variable domains[47,48]. This resulted in maps with 2.9 and 3.0 Å for the monomer and dimer, respectively.

To obtain a higher number of “good” particles, template-based picking was performed in Relion by first generating 2D classes using the monomer particle stack. 2.4 million particles were selected and subjected to rounds of 2D class averaging and 3D refinement as above. Following CTF refinement and Bayesian polishing in Relion of the best class of PhuR monomers, non-uniform refinement in cryoSPARC produced a 2.6 Å

map. This map was subjected to local refinement in cryoSPARC using a tight mask around PhuR and the sAB variable region prepared in Chimera (v1.15), which produced a 2.5 Å map. Local resolution maps were prepared in cryoSPARC and visualized using ChimeraX (v1.5)[49,50]. The detailed data processing workflow is shown in **Supplemental Fig. 4**. Resolutions are reported based on the Fourier Shell Correlation (FSC) equals 0.143 criterion.

Structural model building and refinement

The *B*-factor sharpened map from the cryoSPARC local refinement job was used for model building of the PhuR-sAB11 complex. The AlphaFold model of PhuR was used as the starting coordinates, and manually adjusted into the cryo-EM density map using Chimera. The manually adjusted model and map were then brought into Coot (v0.9) and further adjusted into the density using morphing[51]. The sAB variable region was built using a template (5BJZ) with the CDRs removed, and the sAB11 CDRs were manually built in Coot using the sequence and cryo-EM density to guide manual fitting. PhuR residues without experimental cryo-EM density were deleted. Heme and the lipopolysaccharide (LPS) were built in Coot by manual adjustment into the density. Coordinates for heme were obtained from the Refmac ligand library, and LPS coordinates were obtained from PubChem[52,53]. The LPS headgroup was truncated to the first KDO sugar due to the absence of cryo-EM density for this region. The combined PhuR-sAB model with bound ligands was subjected to multiple rounds of refinement in Coot and Phenix (v1.20), with the map sharpened or blurred in Coot to facilitate model building[54]. The model was inspected manually after each cycle, and refinement was performed until no further

improvement was observed. Waters were added into non-protein and non-ligand densities using Douse and manually inspected. The models were validated in Phenix using its comprehensive cryo-EM validation tools, MolProbity, and EMRinger[55,56]. Directional anisotropy of the map was evaluated using 3DFSC[57].

Structural Analyses

Protein surface interactions were calculated using the Proteins, Interfaces, Structures, and Assemblies server and visualized using PyMol[58]. Consurf was used to analyze evolutionary conservation using the PhuR structure[59,60]. Cavities were analyzed using the Voss Volume Voxelator online tool (http://3vee.molmovdb.org/)[61]. All other images were prepared using Chimera and ChimeraX.

FIGURE LEGENDS

Figure 1: sAB generation and validation **A.** Single point phage ELISA comparing binding of unique clones to PhuR-containing nanodiscs and empty nanodiscs as a control. **B.** Single-point ELISA signal of purified selected sAB clones from the initial phage pool (panel A). Binding of 300 nM of purified sABs tested using PhuR-containing nanodiscs (green), empty nanodiscs (raspberry pink), and a buffer only control (purple). **C.** Affinity estimation ELISA for select sABs measuring binding to PhuR-containing nanodiscs. Data are background subtracted and normalized. Plots are fitted using a nonlinear regression model with variable slope in Prism 9.0 to determine EC_{50}.

Figure 2: CryoEM structure of PhuR-sAB11 complex **A.** Cryo-EM density map of PhuR (jade) bound to sAB11 (heavy chain (HC) shown in orange and light chain (LC) in golden brown) and LPS (mustard). Regions excluded from the model are white. **B.** Front and side views of PhuR-sAB11 complex with LPS and bound heme (raspberry pink) shown. The complex is colored as in A. The conserved loop (CL, purple) with heme-coordinating T529 colored purple. **C.** Side view of LPS and PhuR residues potentially interacting with it. **D.** Top view of LPS KDO sugar and Lipid A headgroup showing conserved interactions with R670 and K721. **E.** Bottom view of LPS tails showing hydrophobic interactions with PhuR. **F.** Close-up view of LC interactions with PhuR. **G.** Close-up view of HC complementarity-determining regions (CDRs) 2 and 3 interactions with PhuR.

Figure 3: Heme recognition by PhuR **A.** Side view of PhuR placed in a schematic bilayer with the plug domain (dark gray), bound LPS, conserved loop, and heme visualized. PhuR

dimensions in Å indicated with arrows. ES - extracellular space, OM - outer membrane, PS - periplasmic space. **B.** Residues involved in the heme (raspberry pink) interaction, including the coordinating Y529. Plug domain and conserved extracellular loop colored dark gray and purple, respectively. **C.** Heme binding site overlaid with cryo-EM density map (gray mesh) contoured to visualize the model and proximal water molecules. **D.** PhuR cryo-EM structure colored according to evolutionary conservation scores of individual residues[59,60]. Legend for conservation scores shown below structure. **E.** Close-up view of heme binding site to show conservation of interacting residues. **F.** Conservation of heme-binding extracellular loop and plug domain shown with bound heme. **G.** Overlay of plug domain structures of PhuR (this study), ShuA (3FHH), and BtuB (1NQG) to compare conformations of the heme binding loop. Heme molecule in PhuR structure shown and colored as above. **H.** Overlay of conserved extracellular loops from the same three structures to highlight conformational differences.

Figure 4: Visualization of PhuR cavities suggest a potential heme uptake mechanism. **A.** Side view of PhuR protein in cartoon representation with extracellular and periplasmic cavitites shown as transparent volumes. Heme is bound to PhuR in the extracellular cavity 1. The second extracellular cavity is proposed based on biochemical data from a previous study[10]. **B.** Close-up view of extracellular cavity 2 with H124 and Y519 shown as sticks together with the bound heme and coordinating Y529. **C.** Top and **D.** side views of capped PhuR structure in surface representation with heme in magenta. **E.** Side view of second cavity bounded by dashed lines with His124 and Tyr519 represented as sticks showing a narrow channel connecting the two cavities.

Figure 5: Biochemical analysis of refolded PhuR and its interaction with sAB11**. A.** Spectroscopic evalutation of heme binding to refolded PhuR using increasing concentrations of heme, performed in triplicate. Data are plotted using Prism (v9.0) software, with the 95% confidence intervals (orange) and standard error bars shown. **B.** Overlay of chromatograms from size exclusion column (SEC) for refolded PhuR alone (green) and after incubation with heme and sAB11 (blue). **C.** SDS-PAGE gel of elution fractions collected after SEC of refolded PhuR in the presence of heme and sAB11. PhuR is present as two bands due to the heat modifiability property of OM proteins[38]. **D.** Representative ns-EM micrograph of peak fraction from panel B. Scale bar represents 50nm. **E.** 2D class averages of refolded PhuR with sAB11 (green arrows) and heme (left panel) and PhuR alone (right panel). Both samples are reconstituted into amphipols. Scale bar represents 10 nm.

Figure S1: PhuR purification in DDM and nanodisc reconstitution. **A.** SEC profile of DDM solubilized protein using pooled PhuR-containing fractions from initial IMAC purification. **B.** SDS-PAGE gel showing protein-containing fractions from SEC run shown in panel A. PhuR appears as two bands due to the heat-modifiability property of β-barrel outer membrane proteins[38]. M - marker; IN - input followed by fraction number corresponding to panel A X-axis. **C.** SEC profile of PhuR reconstituted into E3D1 nanodiscs, either with and without sAB11. A shift in the retention volume and concomitant increase in signal suggested that a complex with sAB11 was formed. **D.** SDS-PAGE gel showing protein fractions from PhuR-E3D1-sAB complex run from panel C. Samples were prepared

without reducing agent to distinguish MSP-E3D1 and the sAB, which when reduced migrates as two bands of approximately the same MW as MSP.

Figure S2: Secondary structure and thermal stability of native and refolded PhuR. **A.** Far-UV CD spectra of refolded (orange) and native (green) PhuR. Graphs plot molar ellipticity vs. wavelength. **B.** Normalized molar ellipticity at 222 nm plotted as a function of temperature to show thermal stability of native (green) and refolded PhuR (orange). This wavelength was monitored due to its signature for β-barrel proteins. Curves fit using Prism 9.0 to determine melting temperature. Thermal denaturation experiments of refolded and native PhuR showed melting temperature of 65°C and 71°C respectively

Figure S3: Cryo-EM single particle analysis of amphipol-reconstituted PhuR-sAB11-Nb complex. **A.** Cryo-EM 3D reconstruction workflow. Representative micrograph shown with 50 nm scale bar and selected particles are shown in green circles. Select 2D class averages shown for antiparallel dimer of PhuR (left) and monomeric PhuR (right) with sAB and nanobody indicated (top). Arrows show progress of reconstruction. Dashed lines show initial data processing strategy. Solid lines show final reconstruction startegy. **B.** Cryo-EM density map of PhuR colored by local resolution with close-up view of density for bound heme. **C.** Directional Fourier Shell Correlation (FSC) plot showing global FSC (red line) with histogram of directional FSCs (blue bars) and standard deviation from mean FSC[57]. Global resolution reported using the FSC = 0.143 criterion.

Figure S4: Model in map fit of PhuR-sAB11-Nb complex. **A.** Selected β-strands from barrel domain shown as green sticks overlaid with cryo-EM density (green mesh). **B.** Heme ligand overlaid with cryo-EM density and represented as in A. **C.** LPS represented as green sticks and overlaid with cryo-EM and colored as in A.

Figure S5: ConSurf evolutionary analysis of PhuR. **A.** PhuR cryo-EM structure colored according to evolutionary conservation scores of individual residues. Legend for conservation scores shown below structure. **B.** Close-up view of heme binding site to show conservation of interacting residues. **C.** Conservation of heme-binding extracellular loop and plug domain shown with bound heme. **A.** Individual residues from cryo-EM structure of PhuR colored by conservation score. Residues are numbered as in the structure. Residues labeled by predicted surface exposure and functionality as based on ConSurf analysis[59,60].

Supplemental Table 1: CDR sequences for selected sAB clones. Sequences of CDRs diversified in Library E shown here[24]. Number of times that the clone appeared in the final phage pool is shown as repeat number.

Supplemental Table 2: Table of EC_{50} values obtained from affinity-estimation ELISA for selected sAB clones.

Supplemental Table 3: Cryo-EM data processing statistics.

REFERENCES

(1) Ferguson, A. D.; Deisenhofer, J. TonB-Dependent Receptors-Structural Perspectives. *Biochim Biophys Acta* **2002**, *1565* (2), 318–332. https://doi.org/10.1016/s0005-2736(02)00578-3.

(2) Silale, A.; Van Den Berg, B. TonB-Dependent Transport Across the Bacterial Outer Membrane. *Annu. Rev. Microbiol.* **2023**, *77* (1), annurev-micro-032421-111116. https://doi.org/10.1146/annurev-micro-032421-111116.

(3) Noinaj, N.; Guillier, M.; Barnard, T. J.; Buchanan, S. K. TonB-Dependent Transporters: Regulation, Structure, and Function. *Annu. Rev. Microbiol.* **2010**, *64* (1), 43–60. https://doi.org/10.1146/annurev.micro.112408.134247.

(4) Krewulak, K. D.; Vogel, H. J. TonB or Not TonB: Is That the Question? *Biochem. Cell Biol.* **2011**, *89* (2), 87–97. https://doi.org/10.1139/O10-141.

(5) Braun, V.; Ratliff, A. C.; Celia, H.; Buchanan, S. K. Energization of Outer Membrane Transport by the ExbB ExbD Molecular Motor. *J Bacteriol* **2023**, *205* (6), e0003523. https://doi.org/10.1128/jb.00035-23.

(6) Ferguson, A. D.; Amezcua, C. A.; Halabi, N. M.; Chelliah, Y.; Rosen, M. K.; Ranganathan, R.; Deisenhofer, J. Signal Transduction Pathway of TonB-Dependent Transporters. *Proc. Natl. Acad. Sci. U.S.A.* **2007**, *104* (2), 513–518. https://doi.org/10.1073/pnas.0609887104.

(7) Krewulak, K. D.; Vogel, H. J. Structural Biology of Bacterial Iron Uptake. *Biochimica et Biophysica Acta (BBA) - Biomembranes* **2008**, *1778* (9), 1781–1804. https://doi.org/10.1016/j.bbamem.2007.07.026.

(8) Hare, S. A. Diverse Structural Approaches to Haem Appropriation by Pathogenic Bacteria. *Biochimica et Biophysica Acta (BBA) - Proteins and Proteomics* **2017**, *1865* (4), 422–433. https://doi.org/10.1016/j.bbapap.2017.01.006.

(9) Smith, A. D.; Wilks, A. Differential Contributions of the Outer Membrane Receptors PhuR and HasR to Heme Acquisition in Pseudomonas Aeruginosa. *J Biol Chem* **2015**, *290* (12), 7756–7766. https://doi.org/10.1074/jbc.M114.633495.

(10) Smith, A. D.; Modi, A. R.; Sun, S.; Dawson, J. H.; Wilks, A. Spectroscopic Determination of Distinct Heme Ligands in Outer-Membrane Receptors PhuR and HasR of Pseudomonas Aeruginosa. *Biochemistry* **2015**, *54* (16), 2601–2612. https://doi.org/10.1021/acs.biochem.5b00017.

(11) Dent, A. T.; Wilks, A. Contributions of the Heme Coordinating Ligands of the Pseudomonas Aeruginosa Outer Membrane Receptor HasR to Extracellular Heme Sensing and Transport. *J Biol Chem* **2020**, *295* (30), 10456–10467. https://doi.org/10.1074/jbc.RA120.014081.

(12) Krieg, S.; Huché, F.; Diederichs, K.; Izadi-Pruneyre, N.; Lecroisey, A.; Wandersman, C.; Delepelaire, P.; Welte, W. Heme Uptake across the Outer Membrane as Revealed by Crystal Structures of the Receptor–Hemophore Complex. *Proc. Natl. Acad. Sci. U.S.A.* **2009**, *106* (4), 1045–1050. https://doi.org/10.1073/pnas.0809406106.

(13) Mouriño, S.; Wilks, A. Extracellular Haem Utilization by the Opportunistic Pathogen Pseudomonas Aeruginosa and Its Role in Virulence and Pathogenesis. In *Advances in Microbial Physiology*; Elsevier, 2021; Vol. 79, pp 89–132. https://doi.org/10.1016/bs.ampbs.2021.07.004.

(14) Marvig, R. L.; Damkiær, S.; Khademi, S. M. H.; Markussen, T. M.; Molin, S.; Jelsbak, L. Within-Host Evolution of Pseudomonas Aeruginosa Reveals Adaptation toward Iron Acquisition from Hemoglobin. *mBio* **2014**, *5* (3), e00966-00914. https://doi.org/10.1128/mBio.00966-14.
(15) Herzik, M. A.; Wu, M.; Lander, G. C. High-Resolution Structure Determination of Sub-100 KDa Complexes Using Conventional Cryo-EM. *Nat Commun* **2019**, *10* (1), 1032. https://doi.org/10.1038/s41467-019-08991-8.
(16) Wentinck, K.; Gogou, C.; Meijer, D. H. Putting on Molecular Weight: Enabling Cryo-EM Structure Determination of Sub-100-KDa Proteins. *Curr Res Struct Biol* **2022**, *4*, 332–337. https://doi.org/10.1016/j.crstbi.2022.09.005.
(17) Dominik, P. K.; Kossiakoff, A. A. Phage Display Selections for Affinity Reagents to Membrane Proteins in Nanodiscs. *Methods Enzymol* **2015**, *557*, 219–245. https://doi.org/10.1016/bs.mie.2014.12.032.
(18) Dominik, P. K.; Borowska, M. T.; Dalmas, O.; Kim, S. S.; Perozo, E.; Keenan, R. J.; Kossiakoff, A. A. Conformational Chaperones for Structural Studies of Membrane Proteins Using Antibody Phage Display with Nanodiscs. *Structure* **2016**, *24* (2), 300–309. https://doi.org/10.1016/j.str.2015.11.014.
(19) Kim, J.; Tan, Y. Z.; Wicht, K. J.; Erramilli, S. K.; Dhingra, S. K.; Okombo, J.; Vendome, J.; Hagenah, L. M.; Giacometti, S. I.; Warren, A. L.; Nosol, K.; Roepe, P. D.; Potter, C. S.; Carragher, B.; Kossiakoff, A. A.; Quick, M.; Fidock, D. A.; Mancia, F. Structure and Drug Resistance of the Plasmodium Falciparum Transporter PfCRT. *Nature* **2019**, *576* (7786), 315–320. https://doi.org/10.1038/s41586-019-1795-x.
(20) Cater, R. J.; Chua, G. L.; Erramilli, S. K.; Keener, J. E.; Choy, B. C.; Tokarz, P.; Chin, C. F.; Quek, D. Q. Y.; Kloss, B.; Pepe, J. G.; Parisi, G.; Wong, B. H.; Clarke, O. B.; Marty, M. T.; Kossiakoff, A. A.; Khelashvili, G.; Silver, D. L.; Mancia, F. Structural Basis of Omega-3 Fatty Acid Transport across the Blood-Brain Barrier. *Nature* **2021**, *595* (7866), 315–319. https://doi.org/10.1038/s41586-021-03650-9.
(21) Ashraf, K. U.; Nygaard, R.; Vickery, O. N.; Erramilli, S. K.; Herrera, C. M.; McConville, T. H.; Petrou, V. I.; Giacometti, S. I.; Dufrisne, M. B.; Nosol, K.; Zinkle, A. P.; Graham, C. L. B.; Loukeris, M.; Kloss, B.; Skorupinska-Tudek, K.; Swiezewska, E.; Roper, D. I.; Clarke, O. B.; Uhlemann, A.-C.; Kossiakoff, A. A.; Trent, M. S.; Stansfeld, P. J.; Mancia, F. Structural Basis of Lipopolysaccharide Maturation by the O-Antigen Ligase. *Nature* **2022**, *604* (7905), 371–376. https://doi.org/10.1038/s41586-022-04555-x.
(22) Feng, P.; Wu, X.; Erramilli, S. K.; Paulo, J. A.; Knejski, P.; Gygi, S. P.; Kossiakoff, A. A.; Rapoport, T. A. A Peroxisomal Ubiquitin Ligase Complex Forms a Retrotranslocation Channel. *Nature* **2022**, *607* (7918), 374–380. https://doi.org/10.1038/s41586-022-04903-x.
(23) Noinaj, N.; Mayclin, S.; Stanley, A. M.; Jao, C. C.; Buchanan, S. K. From Constructs to Crystals – Towards Structure Determination of β-Barrel Outer Membrane Proteins. *JoVE* **2016**, No. 113, 53245. https://doi.org/10.3791/53245.
(24) Miller, K. R.; Koide, A.; Leung, B.; Fitzsimmons, J.; Yoder, B.; Yuan, H.; Jay, M.; Sidhu, S. S.; Koide, S.; Collins, E. J. T Cell Receptor-like Recognition of Tumor in Vivo by Synthetic Antibody Fragment. *PLoS One* **2012**, *7* (8), e43746. https://doi.org/10.1371/journal.pone.0043746.

(25) Paduch, M.; Koide, A.; Uysal, S.; Rizk, S. S.; Koide, S.; Kossiakoff, A. A. Generating Conformation-Specific Synthetic Antibodies to Trap Proteins in Selected Functional States. *Methods* **2013**, *60* (1), 3–14. https://doi.org/10.1016/j.ymeth.2012.12.010.
(26) Zoonens, M.; Popot, J.-L. Amphipols for Each Season. *J Membr Biol* **2014**, *247* (9–10), 759–796. https://doi.org/10.1007/s00232-014-9666-8.
(27) Tsutsumi, N.; Mukherjee, S.; Waghray, D.; Janda, C. Y.; Jude, K. M.; Miao, Y.; Burg, J. S.; Aduri, N. G.; Kossiakoff, A. A.; Gati, C.; Garcia, K. C. Structure of Human Frizzled5 by Fiducial-Assisted Cryo-EM Supports a Heterodimeric Mechanism of Canonical Wnt Signaling. *eLife* **2020**, *9*, e58464. https://doi.org/10.7554/eLife.58464.
(28) Jumper, J.; Evans, R.; Pritzel, A.; Green, T.; Figurnov, M.; Ronneberger, O.; Tunyasuvunakool, K.; Bates, R.; Žídek, A.; Potapenko, A.; Bridgland, A.; Meyer, C.; Kohl, S. A. A.; Ballard, A. J.; Cowie, A.; Romera-Paredes, B.; Nikolov, S.; Jain, R.; Adler, J.; Back, T.; Petersen, S.; Reiman, D.; Clancy, E.; Zielinski, M.; Steinegger, M.; Pacholska, M.; Berghammer, T.; Bodenstein, S.; Silver, D.; Vinyals, O.; Senior, A. W.; Kavukcuoglu, K.; Kohli, P.; Hassabis, D. Highly Accurate Protein Structure Prediction with AlphaFold. *Nature* **2021**, *596* (7873), 583–589. https://doi.org/10.1038/s41586-021-03819-2.
(29) Chimento, D. P.; Kadner, R. J.; Wiener, M. C. Comparative Structural Analysis of TonB-Dependent Outer Membrane Transporters: Implications for the Transport Cycle. *Proteins* **2005**, *59* (2), 240–251. https://doi.org/10.1002/prot.20416.
(30) Chimento, D. P.; Mohanty, A. K.; Kadner, R. J.; Wiener, M. C. Substrate-Induced Transmembrane Signaling in the Cobalamin Transporter BtuB. *Nat Struct Biol* **2003**, *10* (5), 394–401. https://doi.org/10.1038/nsb914.
(31) Sarver, J. L.; Zhang, M.; Liu, L.; Nyenhuis, D.; Cafiso, D. S. A Dynamic Protein–Protein Coupling between the TonB-Dependent Transporter FhuA and TonB. *Biochemistry* **2018**, *57* (6), 1045–1053. https://doi.org/10.1021/acs.biochem.7b01223.
(32) Cobessi, D.; Meksem, A.; Brillet, K. Structure of the Heme/Hemoglobin Outer Membrane Receptor ShuA from *Shigella Dysenteriae* : Heme Binding by an Induced Fit Mechanism. *Proteins* **2010**, *78* (2), 286–294. https://doi.org/10.1002/prot.22539.
(33) Buchanan, S. K.; Lukacik, P.; Grizot, S.; Ghirlando, R.; Ali, M. M. U.; Barnard, T. J.; Jakes, K. S.; Kienker, P. K.; Esser, L. Structure of Colicin I Receptor Bound to the R-Domain of Colicin Ia: Implications for Protein Import. *EMBO J* **2007**, *26* (10), 2594–2604. https://doi.org/10.1038/sj.emboj.7601693.
(34) Buchanan, S. K.; Smith, B. S.; Venkatramani, L.; Xia, D.; Esser, L.; Palnitkar, M.; Chakraborty, R.; van der Helm, D.; Deisenhofer, J. Crystal Structure of the Outer Membrane Active Transporter FepA from Escherichia Coli. *Nat Struct Biol* **1999**, *6* (1), 56–63. https://doi.org/10.1038/4931.
(35) Cobessi, D.; Celia, H.; Pattus, F. Crystal Structure at High Resolution of Ferric-Pyochelin and Its Membrane Receptor FptA from Pseudomonas Aeruginosa. *J Mol Biol* **2005**, *352* (4), 893–904. https://doi.org/10.1016/j.jmb.2005.08.004.
(36) Mokry, D. Z.; Nadia-Albete, A.; Johnson, M. K.; Lukat-Rodgers, G. S.; Rodgers, K. R.; Lanzilotta, W. N. Spectroscopic Evidence for a 5-Coordinate Oxygenic Ligated High Spin Ferric Heme Moiety in the Neisseria Meningitidis Hemoglobin Binding Receptor. *Biochimica et Biophysica Acta (BBA) - General Subjects* **2014**, *1840* (10), 3058–3066. https://doi.org/10.1016/j.bbagen.2014.06.009.

(37) Storek, K. M.; Chan, J.; Vij, R.; Chiang, N.; Lin, Z.; Bevers, J.; Koth, C. M.; Vernes, J.-M.; Meng, Y. G.; Yin, J.; Wallweber, H.; Dalmas, O.; Shriver, S.; Tam, C.; Schneider, K.; Seshasayee, D.; Nakamura, G.; Smith, P. A.; Payandeh, J.; Koerber, J. T.; Comps-Agrar, L.; Rutherford, S. T. Massive Antibody Discovery Used to Probe Structure–Function Relationships of the Essential Outer Membrane Protein LptD. *eLife* **2019**, *8*, e46258. https://doi.org/10.7554/eLife.46258.
(38) Noinaj, N.; Kuszak, A. J.; Buchanan, S. K. Heat Modifiability of Outer Membrane Proteins from Gram-Negative Bacteria. *Methods Mol Biol* **2015**, *1329*, 51–56. https://doi.org/10.1007/978-1-4939-2871-2_4.
(39) Alvarez, F. J. D.; Orelle, C.; Davidson, A. L. Functional Reconstitution of an ABC Transporter in Nanodiscs for Use in Electron Paramagnetic Resonance Spectroscopy. *J Am Chem Soc* **2010**, *132* (28), 9513–9515. https://doi.org/10.1021/ja104047c.
(40) Erramilli, S. K.; Dominik, P. K.; Deneka, D.; Tokarz, P.; Kim, S. S.; Reddy, B. G.; Skrobek, B. M.; Dalmas, O.; Perozo, E.; Kossiakoff, A. A. Conformation-Specific Synthetic Antibodies Discriminate Multiple Functional States of the Ion Channel CorA. *Journal of Molecular Biology* **2023**, *435* (17), 168192. https://doi.org/10.1016/j.jmb.2023.168192.
(41) Zivanov, J.; Nakane, T.; Forsberg, B. O.; Kimanius, D.; Hagen, W. J.; Lindahl, E.; Scheres, S. H. New Tools for Automated High-Resolution Cryo-EM Structure Determination in RELION-3. *Elife* **2018**, *7*, e42166. https://doi.org/10.7554/eLife.42166.
(42) Morin, A.; Eisenbraun, B.; Key, J.; Sanschagrin, P. C.; Timony, M. A.; Ottaviano, M.; Sliz, P. Collaboration Gets the Most out of Software. *Elife* **2013**, *2*, e01456. https://doi.org/10.7554/eLife.01456.
(43) Punjani, A.; Rubinstein, J. L.; Fleet, D. J.; Brubaker, M. A. CryoSPARC: Algorithms for Rapid Unsupervised Cryo-EM Structure Determination. *Nat Methods* **2017**, *14* (3), 290–296. https://doi.org/10.1038/nmeth.4169.
(44) Zheng, S. Q.; Palovcak, E.; Armache, J.-P.; Verba, K. A.; Cheng, Y.; Agard, D. A. MotionCor2: Anisotropic Correction of Beam-Induced Motion for Improved Cryo-Electron Microscopy. *Nat Methods* **2017**, *14* (4), 331–332. https://doi.org/10.1038/nmeth.4193.
(45) Scheres, S. H. W. RELION: Implementation of a Bayesian Approach to Cryo-EM Structure Determination. *Journal of Structural Biology* **2012**, *180* (3), 519–530. https://doi.org/10.1016/j.jsb.2012.09.006.
(46) Zhang, K. Gctf: Real-Time CTF Determination and Correction. *J Struct Biol* **2016**, *193* (1), 1–12. https://doi.org/10.1016/j.jsb.2015.11.003.
(47) Zivanov, J.; Nakane, T.; Scheres, S. H. W. A Bayesian Approach to Beam-Induced Motion Correction in Cryo-EM Single-Particle Analysis. *IUCrJ* **2019**, *6* (Pt 1), 5–17. https://doi.org/10.1107/S205225251801463X.
(48) Asarnow, D.; Palovcak, E.; Cheng, Y. Asarnow/Pyem: UCSF Pyem v0.5, 2019. https://doi.org/10.5281/ZENODO.3576630.
(49) Pettersen, E. F.; Goddard, T. D.; Huang, C. C.; Couch, G. S.; Greenblatt, D. M.; Meng, E. C.; Ferrin, T. E. UCSF Chimera--a Visualization System for Exploratory Research and Analysis. *J Comput Chem* **2004**, *25* (13), 1605–1612. https://doi.org/10.1002/jcc.20084.
(50) Pettersen, E. F.; Goddard, T. D.; Huang, C. C.; Meng, E. C.; Couch, G. S.; Croll, T. I.; Morris, J. H.; Ferrin, T. E. UCSF ChimeraX: Structure Visualization for Researchers, Educators, and Developers. *Protein Sci* **2021**, *30* (1), 70–82. https://doi.org/10.1002/pro.3943.

(51) Emsley, P.; Cowtan, K. Coot: Model-Building Tools for Molecular Graphics. *Acta Crystallogr D Biol Crystallogr* **2004**, *60* (Pt 12 Pt 1), 2126–2132. https://doi.org/10.1107/S0907444904019158.
(52) Murshudov, G. N.; Skubák, P.; Lebedev, A. A.; Pannu, N. S.; Steiner, R. A.; Nicholls, R. A.; Winn, M. D.; Long, F.; Vagin, A. A. *REFMAC* 5 for the Refinement of Macromolecular Crystal Structures. *Acta Crystallogr D Biol Crystallogr* **2011**, *67* (4), 355–367. https://doi.org/10.1107/S0907444911001314.
(53) Kim, S.; Chen, J.; Cheng, T.; Gindulyte, A.; He, J.; He, S.; Li, Q.; Shoemaker, B. A.; Thiessen, P. A.; Yu, B.; Zaslavsky, L.; Zhang, J.; Bolton, E. E. PubChem 2023 Update. *Nucleic Acids Research* **2023**, *51* (D1), D1373–D1380. https://doi.org/10.1093/nar/gkac956.
(54) Afonine, P. V.; Poon, B. K.; Read, R. J.; Sobolev, O. V.; Terwilliger, T. C.; Urzhumtsev, A.; Adams, P. D. Real-Space Refinement in PHENIX for Cryo-EM and Crystallography. *Acta Crystallogr D Struct Biol* **2018**, *74* (Pt 6), 531–544. https://doi.org/10.1107/S2059798318006551.
(55) Chen, V. B.; Arendall, W. B.; Headd, J. J.; Keedy, D. A.; Immormino, R. M.; Kapral, G. J.; Murray, L. W.; Richardson, J. S.; Richardson, D. C. MolProbity: All-Atom Structure Validation for Macromolecular Crystallography. *Acta Crystallogr D Biol Crystallogr* **2010**, *66* (Pt 1), 12–21. https://doi.org/10.1107/S0907444909042073.
(56) Barad, B. A.; Echols, N.; Wang, R. Y.-R.; Cheng, Y.; DiMaio, F.; Adams, P. D.; Fraser, J. S. EMRinger: Side Chain-Directed Model and Map Validation for 3D Cryo-Electron Microscopy. *Nat Methods* **2015**, *12* (10), 943–946. https://doi.org/10.1038/nmeth.3541.
(57) Tan, Y. Z.; Baldwin, P. R.; Davis, J. H.; Williamson, J. R.; Potter, C. S.; Carragher, B.; Lyumkis, D. Addressing Preferred Specimen Orientation in Single-Particle Cryo-EM through Tilting. *Nat Methods* **2017**, *14* (8), 793–796. https://doi.org/10.1038/nmeth.4347.
(58) Krissinel, E.; Henrick, K. Inference of Macromolecular Assemblies from Crystalline State. *J Mol Biol* **2007**, *372* (3), 774–797. https://doi.org/10.1016/j.jmb.2007.05.022.
(59) Landau, M.; Mayrose, I.; Rosenberg, Y.; Glaser, F.; Martz, E.; Pupko, T.; Ben-Tal, N. ConSurf 2005: The Projection of Evolutionary Conservation Scores of Residues on Protein Structures. *Nucleic Acids Research* **2005**, *33* (Web Server), W299–W302. https://doi.org/10.1093/nar/gki370.
(60) Yariv, B.; Yariv, E.; Kessel, A.; Masrati, G.; Chorin, A. B.; Martz, E.; Mayrose, I.; Pupko, T.; Ben-Tal, N. Using Evolutionary Data to Make Sense of Macromolecules with a "Face-Lifted" ConSurf. *Protein Sci* **2023**, *32* (3), e4582. https://doi.org/10.1002/pro.4582.
(61) Voss, N. R.; Gerstein, M. 3V: Cavity, Channel and Cleft Volume Calculator and Extractor. *Nucleic Acids Research* **2010**, *38* (Web Server), W555–W562. https://doi.org/10.1093/nar/gkq395.

Figure 1

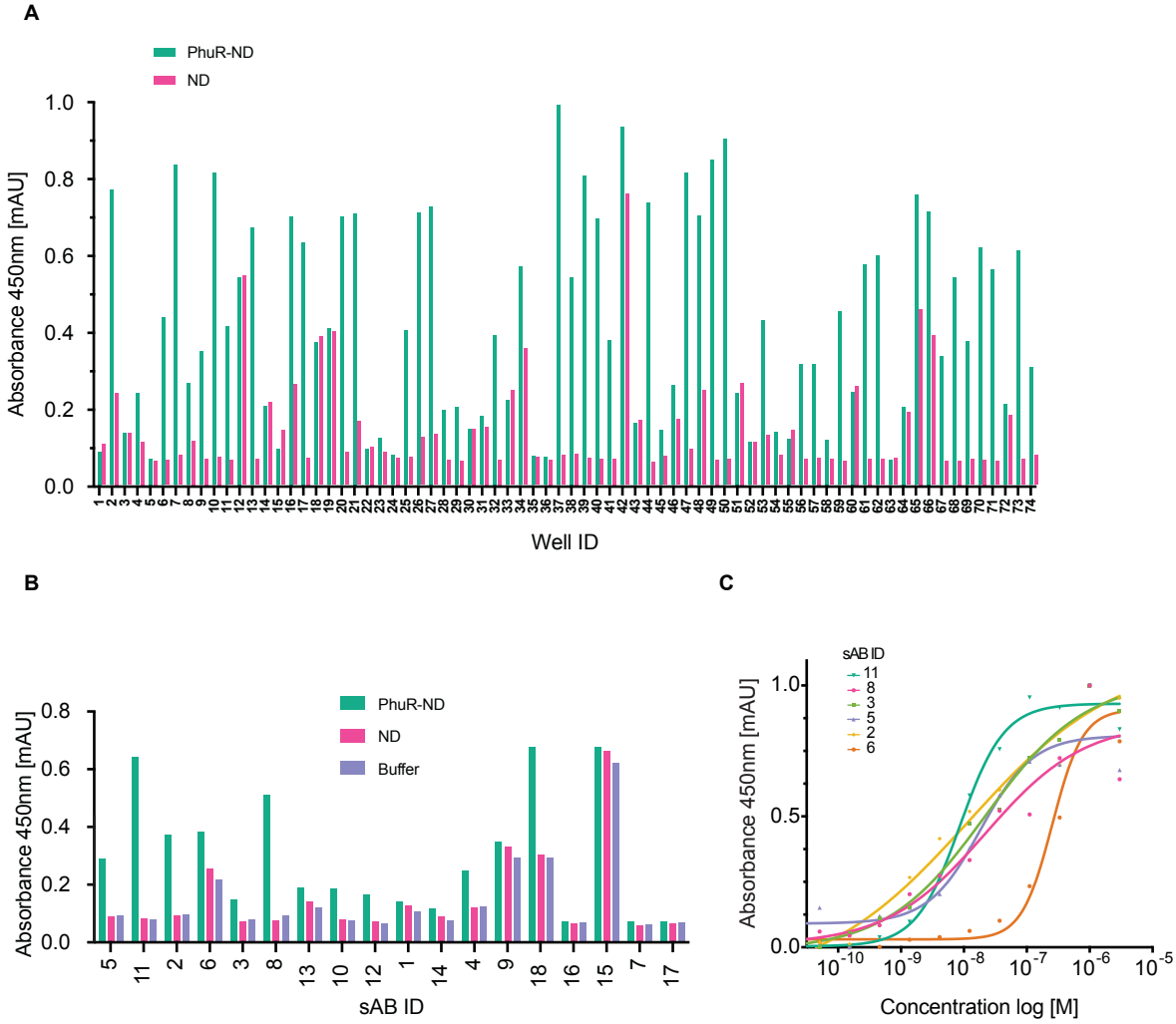
A
PhuR-ND
ND
Absorbance 450nm [mAU]
Well ID
B
PhuR-ND
ND
Buffer
Absorbance 450nm [mAU]
sAB ID
C
sAB ID
11
8
3
5
2
6
Absorbance 450nm [mAU]
Concentration log [M]

Figure 2

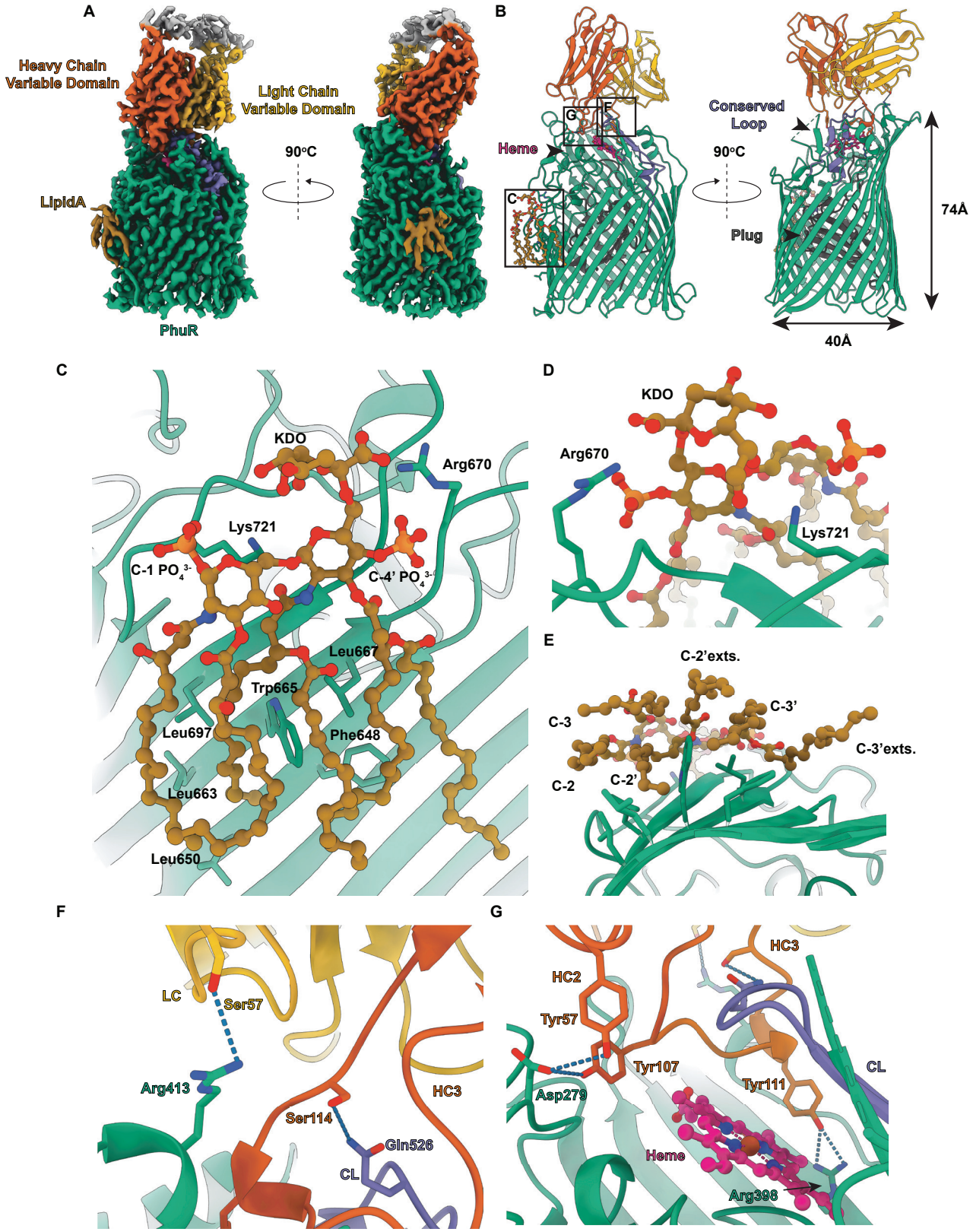
A
Heavy Chain
Variable Domain
Light Chain
Variable Domain
90°C
LipidA
PhuR
B
G
F
Heme
C
Conserved
Loop
90°C
Plug
74Å
40Å
C
KDO
Arg670
Lys721
C-1 PO4 3-
C-4' PO4 3-
Leu667
Trp665
Leu697
Phe648
Leu663
Leu650
D
KDO
Arg670
Lys721
E
C-2'exts.
C-3'
C-3
C-3'exts.
C-2
C-2'
F
LC
Ser57
Arg413
HC3
Ser114
Gln526
CL
G
HC3
HC2
Tyr57
Tyr107
CL
Tyr111
Asp279
Heme
Arg398

Figure 3

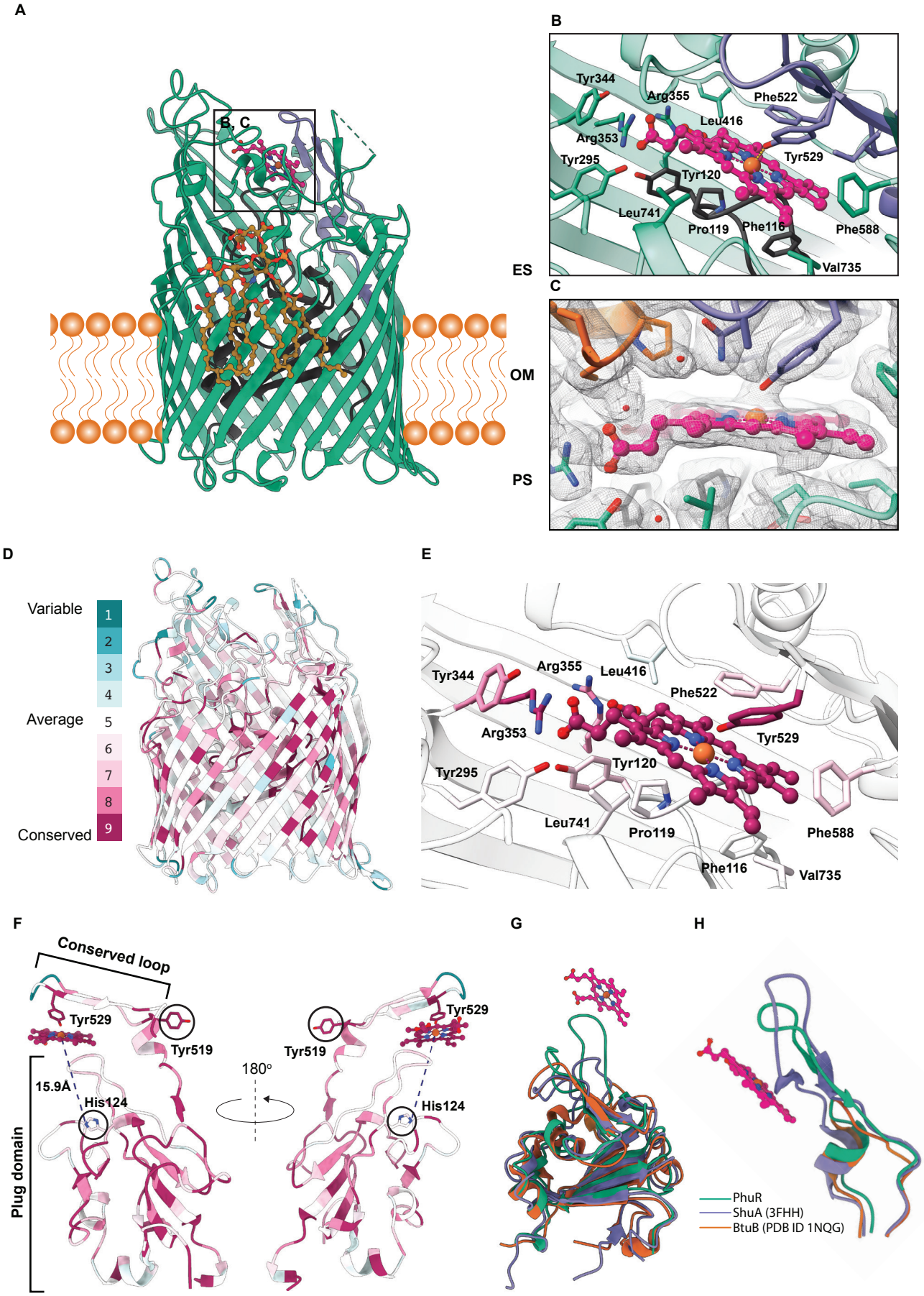
A
B, C
ES
OM
PS
B
Tyr344
Arg355
Phe522
Leu416
Arg353
Tyr529
Tyr295
Tyr120
Leu741
Pro119
Phe116
Phe588
Val735
C
D
Variable
1
2
3
4
Average
5
6
7
8
Conserved
9
E
Tyr344
Arg355
Leu416
Phe522
Arg353
Tyr529
Tyr295
Tyr120
Leu741
Pro119
Phe588
Phe116
Val735
F
Conserved loop
Tyr529
Tyr519
15.9Å
His124
Plug domain
180°
Tyr519
Tyr529
His124
G
H
PhuR
ShuA (3FHH)
BtuB (PDB ID 1NQG)

Figure 4

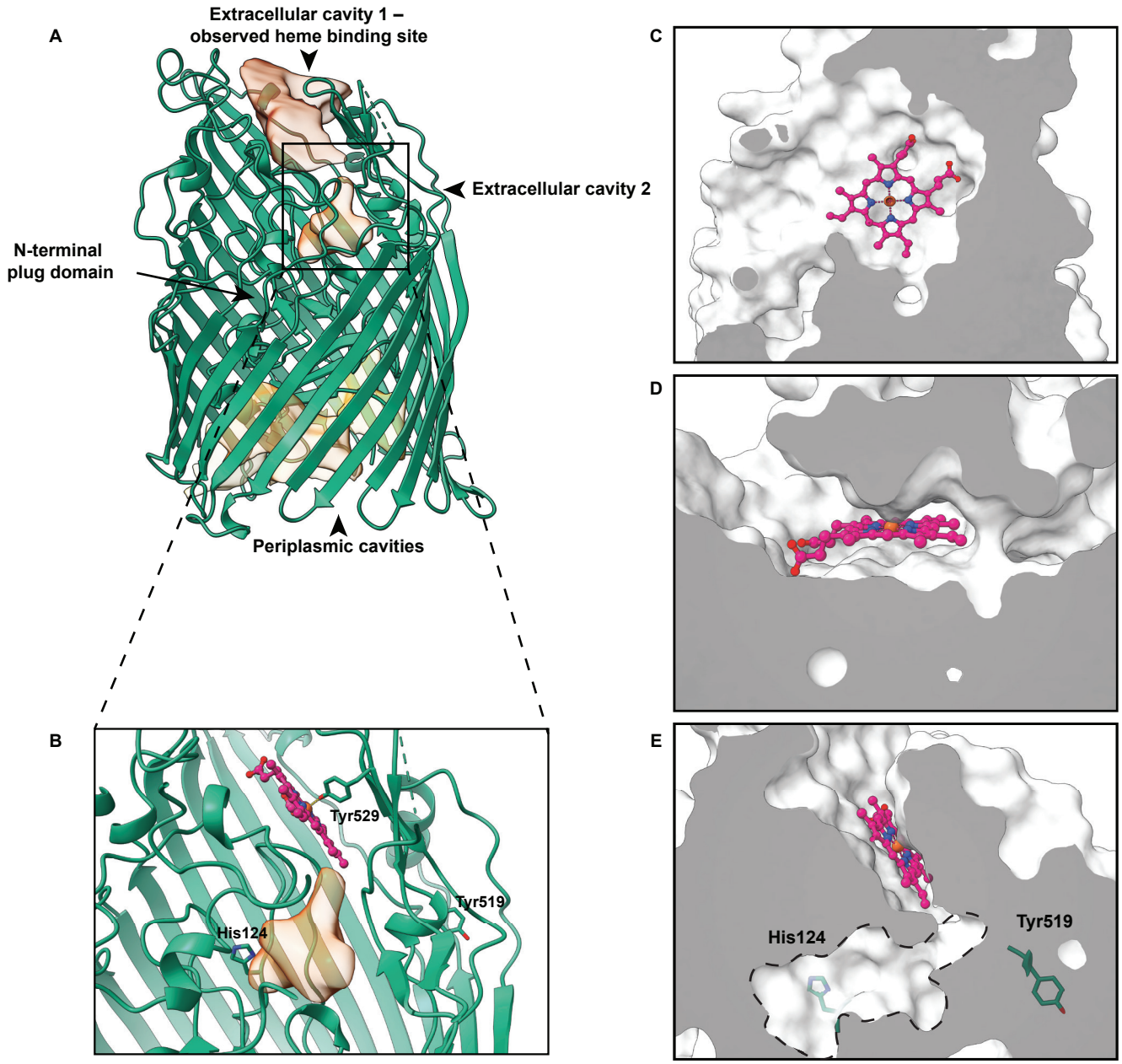
A
Extracellular cavity 1 –
observed heme binding site
Extracellular cavity 2
N-terminal
plug domain
Periplasmic cavities
B
Tyr529
Tyr519
His124
C
D
E
His124
Tyr519

Figure 5

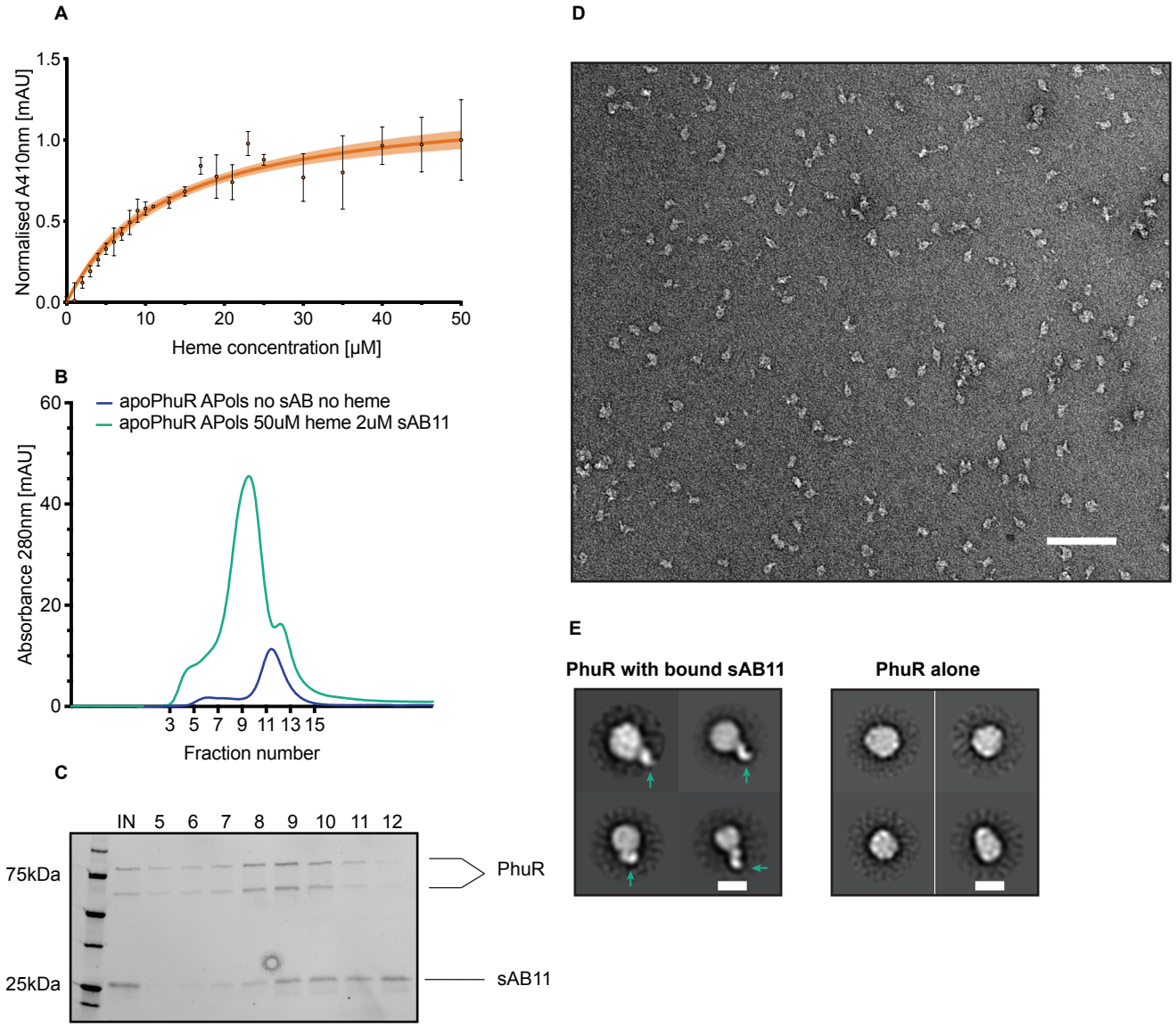
A
Normalised A410nm [mAU]
1.5
1.0
0.5
0.0
0
10
20
30
40
50
Heme concentration [μM]
B
apoPhuR APols no sAB no heme
apoPhuR APols 50uM heme 2uM sAB11
Absorbance 280nm [mAU]
60
40
20
0
3 5 7 9 11 13 15
Fraction number
C
IN 5 6 7 8 9 10 11 12
75kDa
25kDa
PhuR
sAB11
D
E
PhuR with bound sAB11
PhuR alone